Supporting information for

Crystallization and Single Molecule Magnetic Behavior of Quadruple-stranded Helicate: Tuning the Anisotropic Axes †

Xingrui Gao,[a] Li Li,[b] Wenbin Sun*[a] and Peng Chen,*[a]

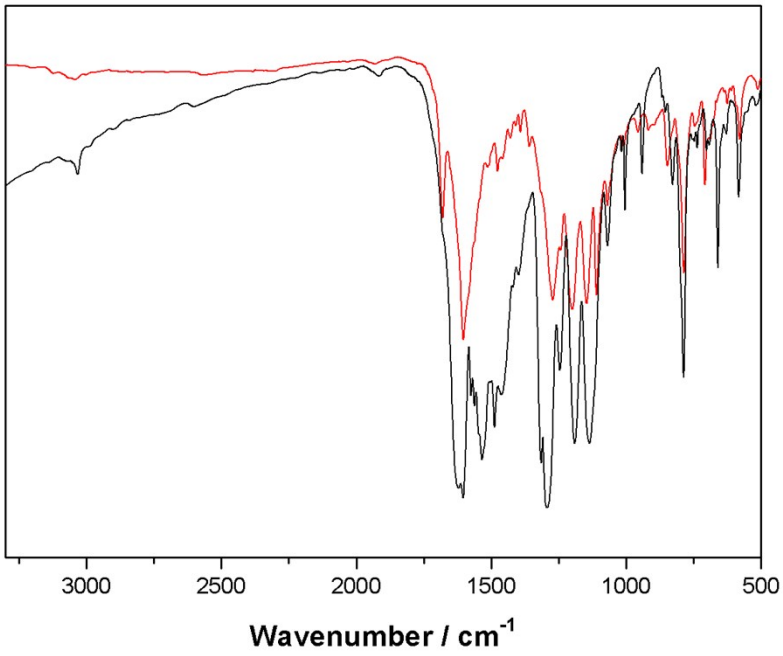

Fig. S1 IR spectra of **2** (black) and BTT (red).

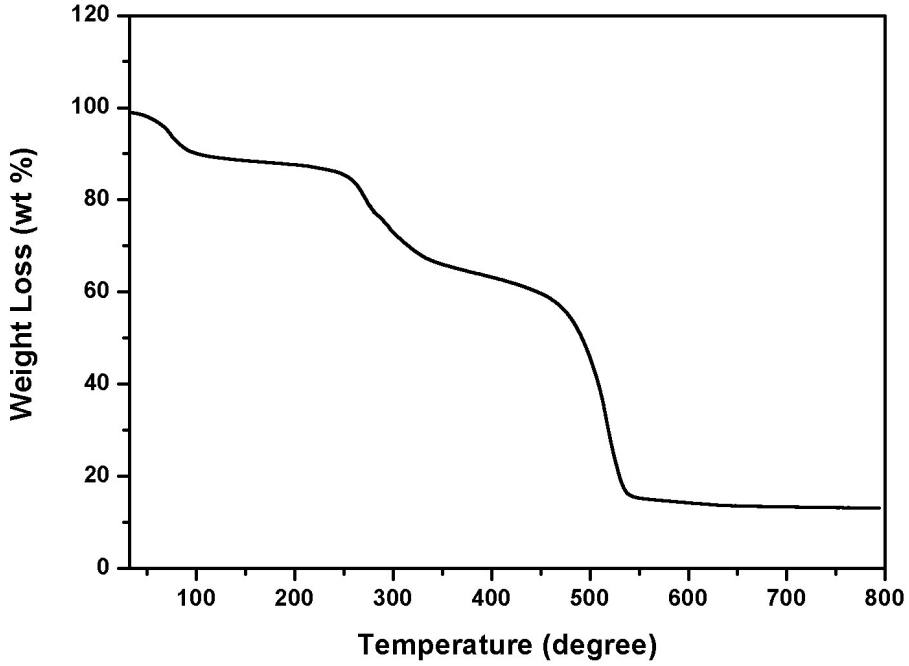

Fig. S2 TG curve of **1**.

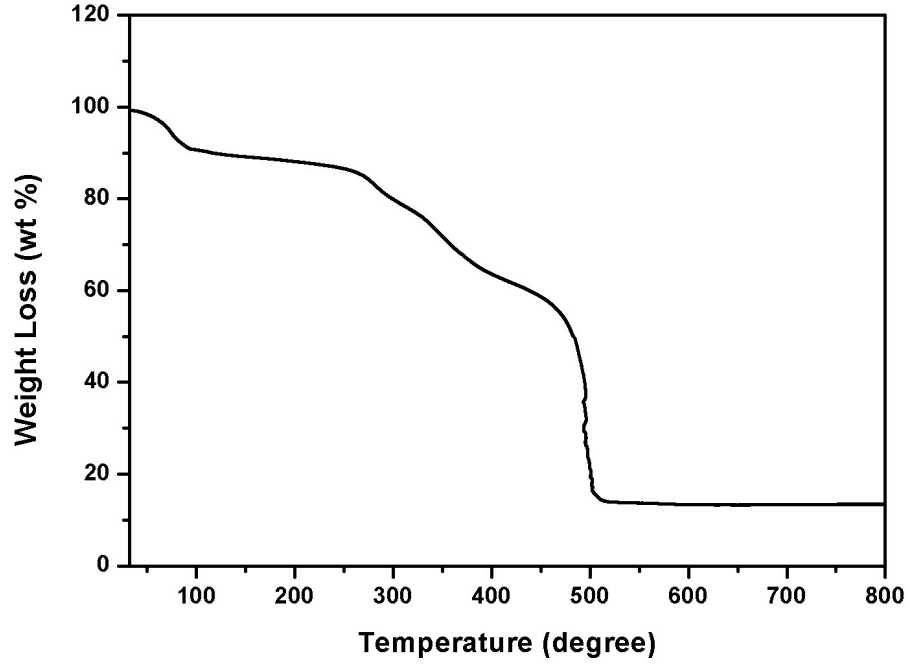

Fig. S3 TG curve of **2**.

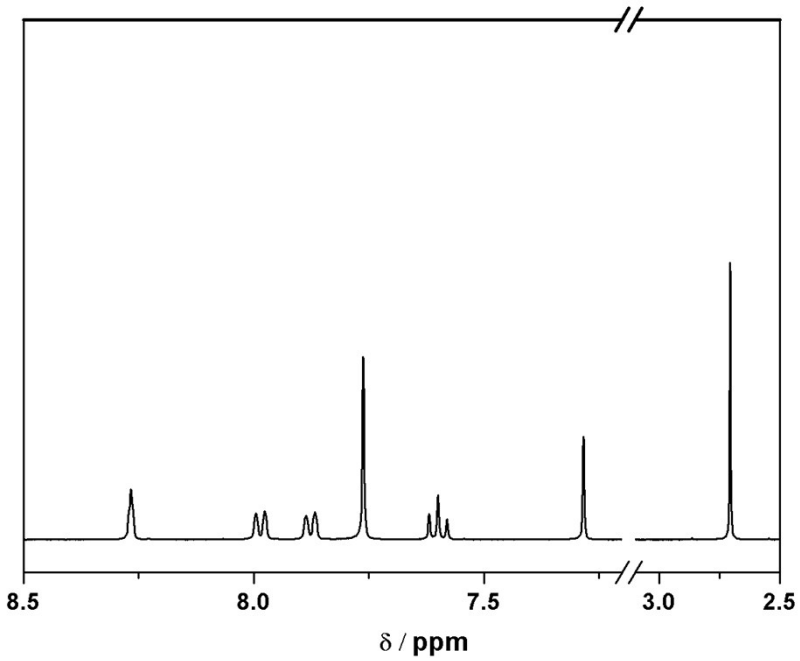

Fig. S4 ^{1}H NMR spectrum of 3,3'-diacetylbiphenylbenzene.

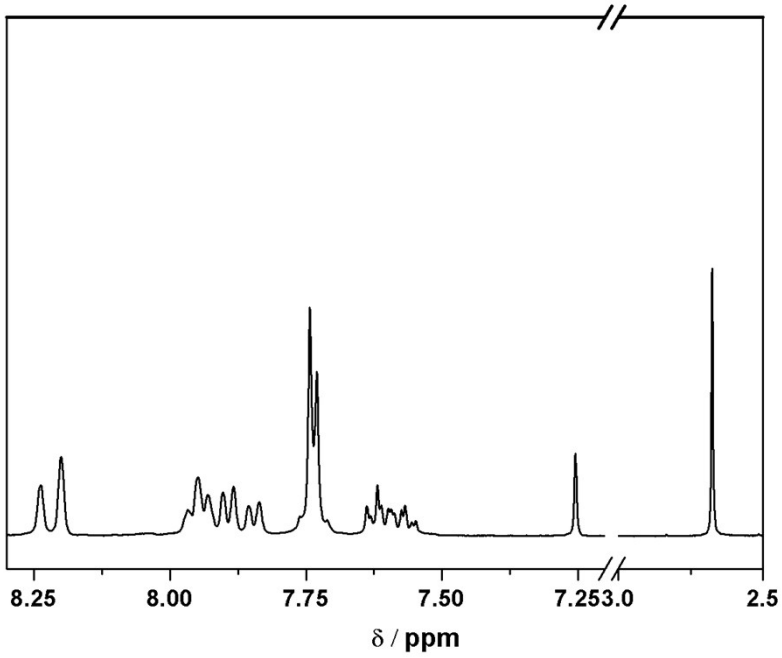

Fig. S5 ^{1}H NMR spectrum of BTT.

Synthesis of 4,4'-diacetyl-*m*-terphenyl

The Suzuki coupling reaction similar to the preparation of 3,3'-diacetylbiphenylbenzene was employed, and the synthetic rout was shown in Scheme S1. It is noted that the product could not be purified with silica gel flash chromatography, since the polarity of the as-synthesized by-product 4,4'-diacetylbiphenyl was similar to that of the target molecule as far as we had tried. Purification by silica gel flash chromatography with ethyl acetate/hexane (1:3) afforded the product as white solid (61 % yield). Anal. Calcd. for $C_{22}H_{18}O_2$ (314.38): C, 84.05; H, 5.77 wt%. Found: C, 84.03; H, 5.79 wt%. IR (KBr, cm^{-1}): 2923 (s), 1674 (s), 1438 (s), 1239 (s), 801 (s). ^1H NMR (400 MHz, $CDCl_3$, 25 ^oC, TMS): δ = 8.06 (d, J = 8.21 Hz, 4H), 7.74 (m, 8H), 2.65 ppm (s, 6H). ^1H NMR spectra of 3,3'-diacetyl-*m*-terphenyl was shown in Fig. S5.

Synthesis of BTT[a]

4,4"-bis(4,4,4-trifluoro-1,3-dioxobutyl)-m-terphenyl (**BTT[a]**) had been similarly prepared. Anal. Calcd. for $C_{26}H_{16}F_6O_4$ (506.10): C, 61.67; H, 3.18. Found: C, 61.66; H, 3.20. IR (KBr, cm^{-1}): 3422 (w), 2923 (w), 1600 (s), 1278 (s), 1183 (s), 1153 (s), 1264 (s), 788 (s). ^1H NMR (400 MHz, $CDCl_3$, 25 ^oC, TMS): δ = 8.06 (d, J = 8.36 Hz, 4H), 7.80-7.73 (m, 8H), 2.65 (s, 2H). ^1H NMR spectra of BTT was shown in Fig. S6.

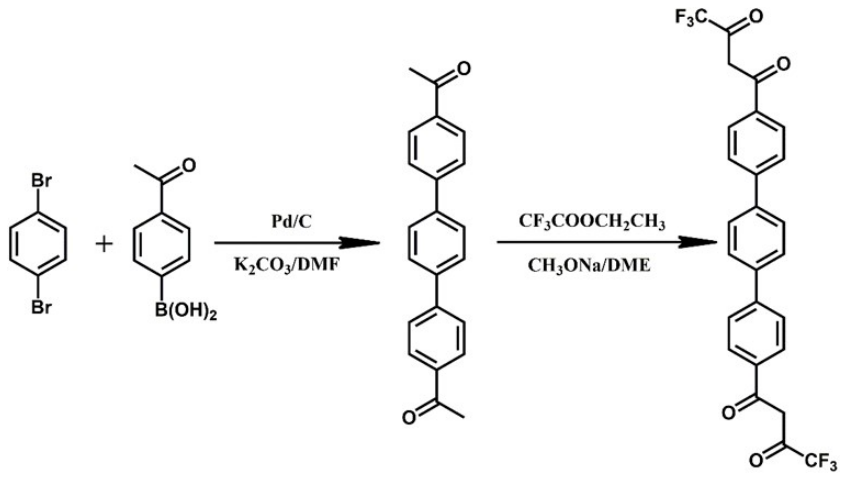

Scheme S1 Synthetic route for BTT[a]

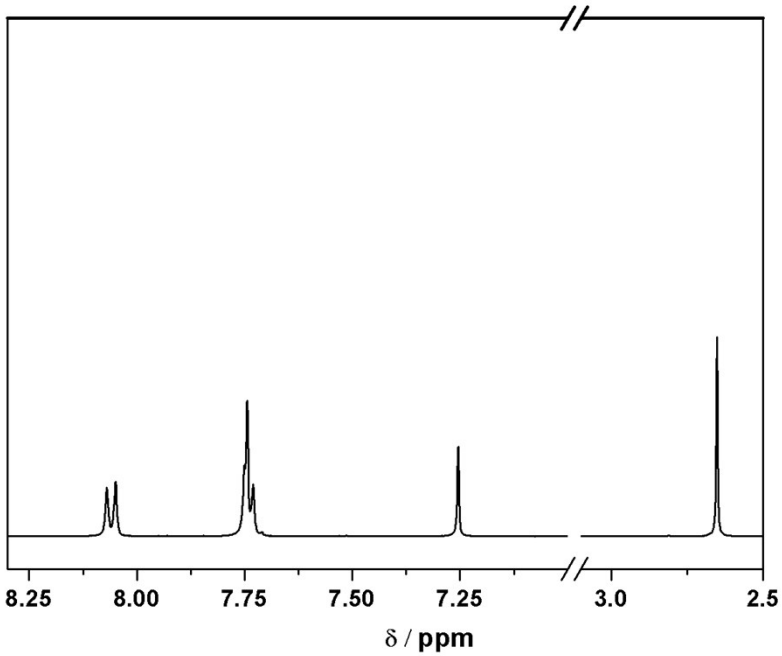

Fig. S6 ^{1}H NMR spectrum of 4,4'-diacetylbiphenylbenzene.

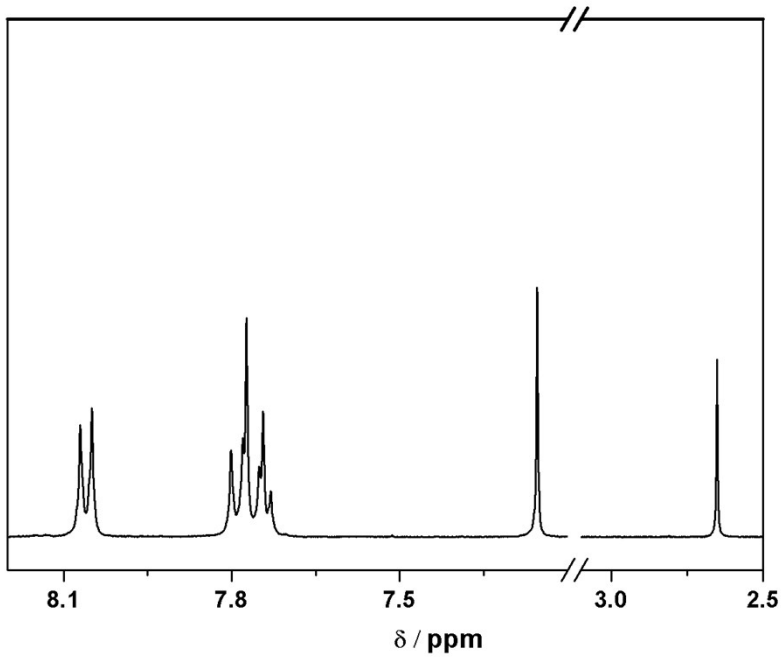

Fig. S7 ^{1}H NMR spectrum of BTT[a].

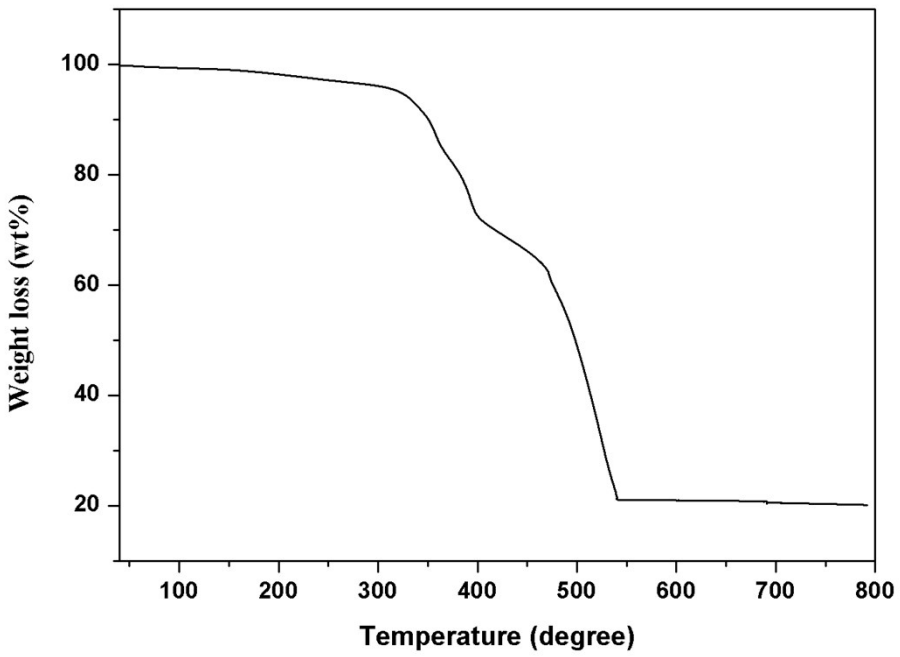

Fig. S8 TG curve of $Dy_2(BTT^a)_3$.

On account of the rigidity and length of the ligand, it is supposed that a triple-stranded helicate could be expected with the assembly of Ln^{3+} ions and BTT^a ligands.[s1-3] The helicate with a general formula of $Dy_2(BTT^a)_3(H_2O)_4$ could be obtained by the similar method once $DyCl_3$ is used. Unlike complexes **1** and **2**, no distinct weight loss occurs around 200 ^oC, which is ascribed to the removal of triethylamine as it is shown in Fig. S7. A residue of 20.09 wt% is found in good accordance with the theoretical value of 19.53 wt%, provided that it is a triple-stranded complex. Before 300 ^oC, an approximate 3.68 wt% (calc. 3.77 wt%) is observed for the removal of hydrates attached the Dy^{3+} ions. Thereafter, a weight loss of 76.28 wt% is in good agreement with the theoretical value for three BTT^a ligand (76.70 wt%).

References:

S1: P. Chen, H. Li, W. Sun, J. Tang, L. Zhang and P. Yan, *CrystEngComm*, 2015, **17**, 7227.

S2: X. Gao, H. Li, P. Chen, W. Sun and P. Yan, *Polyhedron*, 2017, **126**, 1.

S3: H. Li, P. Chen, W. Sun, L. Zhang and P. Yan, *Dalton Trans*., 2016, **45**, 3175

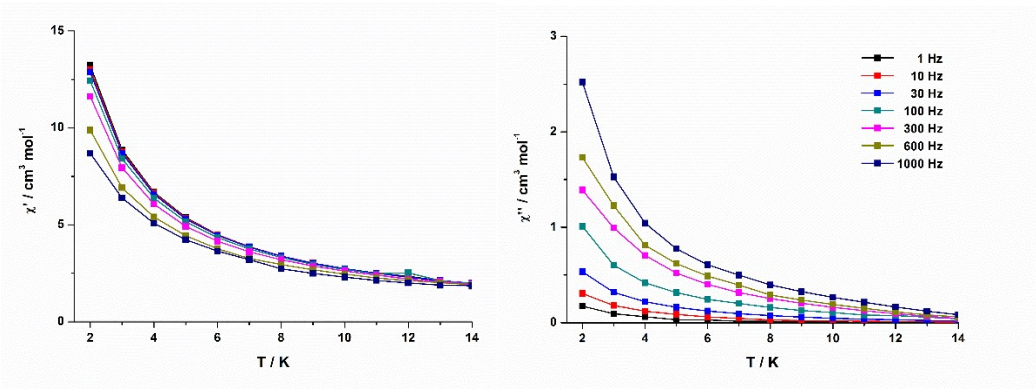

Fig. S9 Temperature dependence of the in-phase (left) and out-of-phase (right) AC susceptibility for **2** under zero DC field.

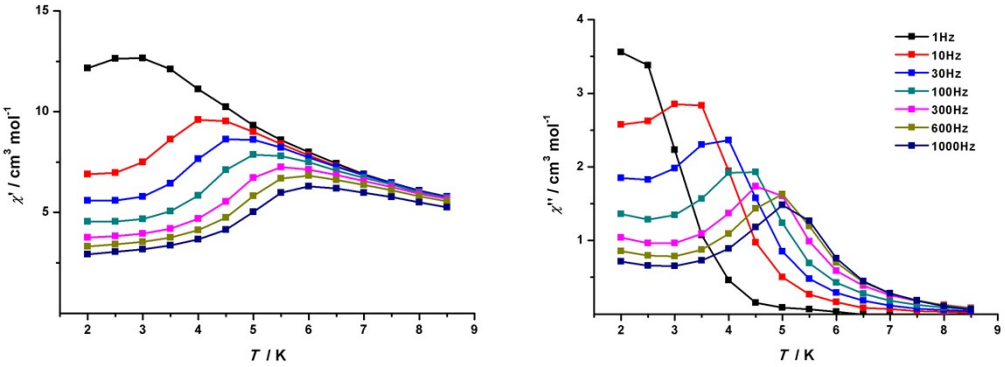

Fig. S10 Temperature dependence of the in-phase (left) and out-of-phase (right) AC susceptibility for **2** under 2000 Oe DC field.

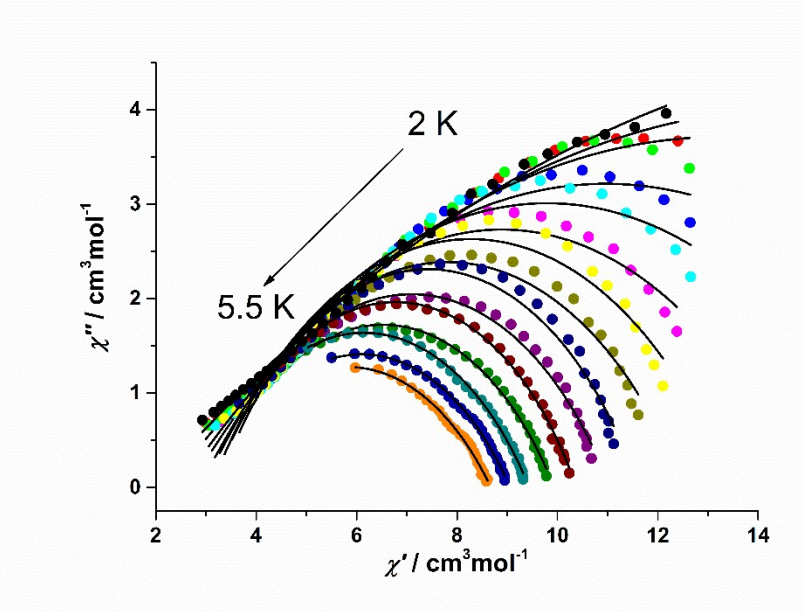

Fig. S11 Cole-Cole plots using the ac susceptibility data of **2** under an applied field of 2000 Oe (2-5.5 K, 0.25K interval).

Table S1 Key geometric parameters for the multiple-stranded helicates in **2**-**8**. (TD: Triangular dodecahedron; SA: Square antiprism)

code	The angle of Dy…Dy and corresponding easy axis of (deg)		Torsion of two easy axes (deg)	Distance of two Dy centers in the same helicate (Å)	Configuration of the Dy centers, calculated by *Shape*[1]	
	Dy1	Dy2			Dy1	Dy2
2	86.5	89.6	60.9	12.9	SA	SA
3[2]	77.5	77.3	38.9	11.9	SA	SA
4[2]	74.4	76.4	17.1	11.9	TD	SA
5[2]	74.2	77.3	30.5	11.9	SA	SA
6[3]	82.0	84.8	55.5	14.3	SA	TD
7[4]	86.6	84.0	46.8	12.6	TD	SA
8[4]	69.8	81.3	0.09	13.4	SA	SA

1. (a) S. Alvarez, P. Alemany, D. Casanova, J. Cirera, M. Llunell and D. Avnir, *Coord. Chem. Rev*., 2005, **249**, 1693;(b) M. Llunell, D. Casanova, J. Cirera, P. Alemany and S. Alvarez, *SHAPE*, v2.1, University of Barcelona and The Hebrew University of Jerusalem, Barcelona and Jerusalem, 2013.
2. H. Li, P. Chen, W. Sun, L. Zhang and P. Yan, *Dalton Trans*., 2016, **45**, 3175.
3. X. Gao, H. Li, P. Chen, W. Sun and P. Yan, *Polyhedron*, 2017, **126**, 1.
4. P. Chen, H. Li, W. Sun, J. Tang, L. Zhang and P. Yan, *CrystEngComm*, 2015, **17**, 7227

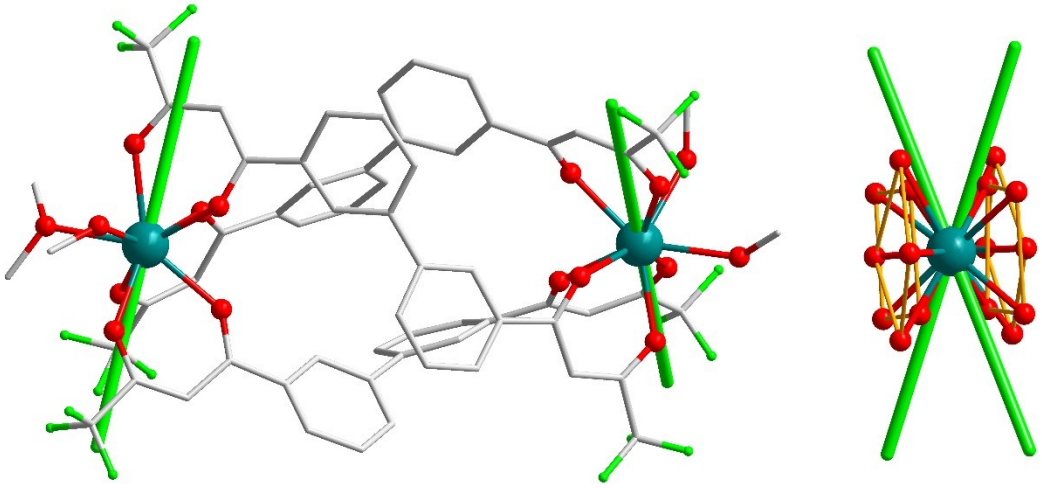

Fig. S12 Magnetic easy axis direction of each Dy(III) ion in **3** (left) and the side view (right).

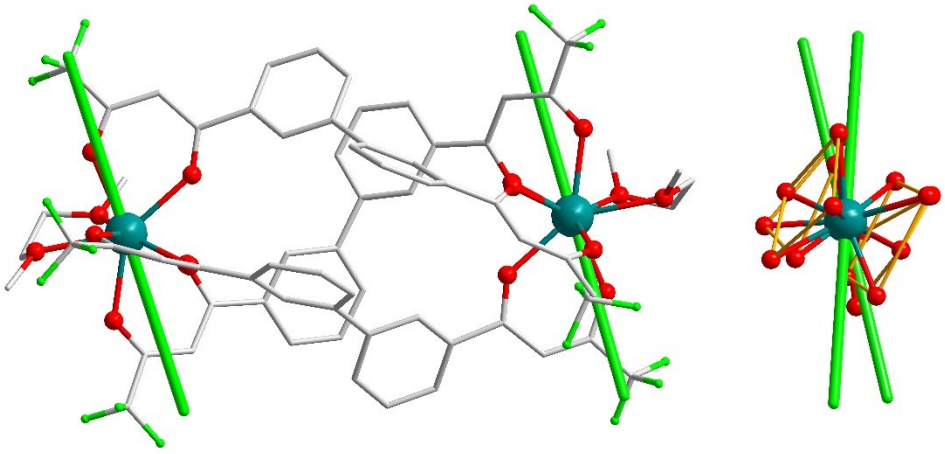

Fig. S13 Magnetic easy axis direction of each Dy(III) ion in **4** (left) and the side view (right).

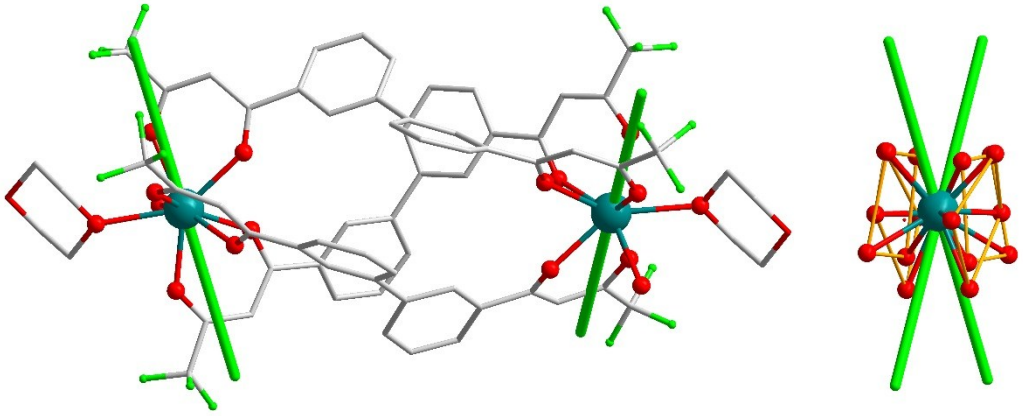

Fig. S14 Magnetic easy axis direction of each Dy(III) ion in **5** (left) and the side view (right).

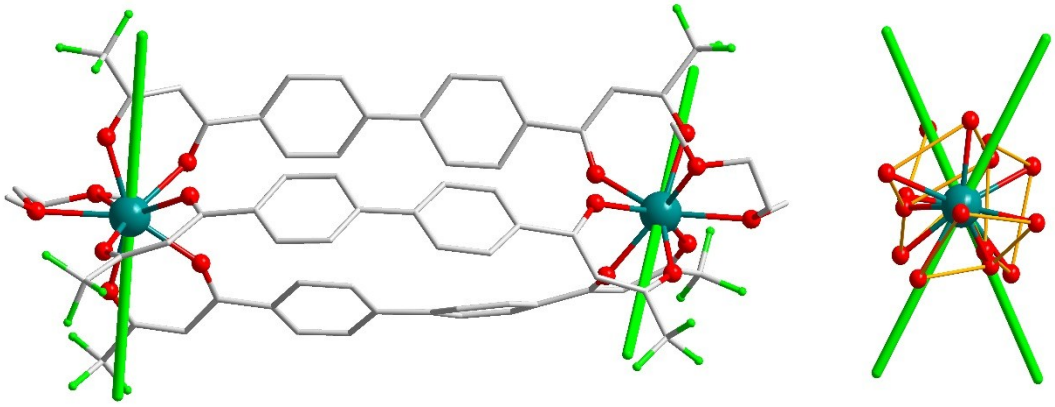

Fig. S15 Magnetic easy axis direction of each Dy(III) ion in **6** (left) and the side view (right).

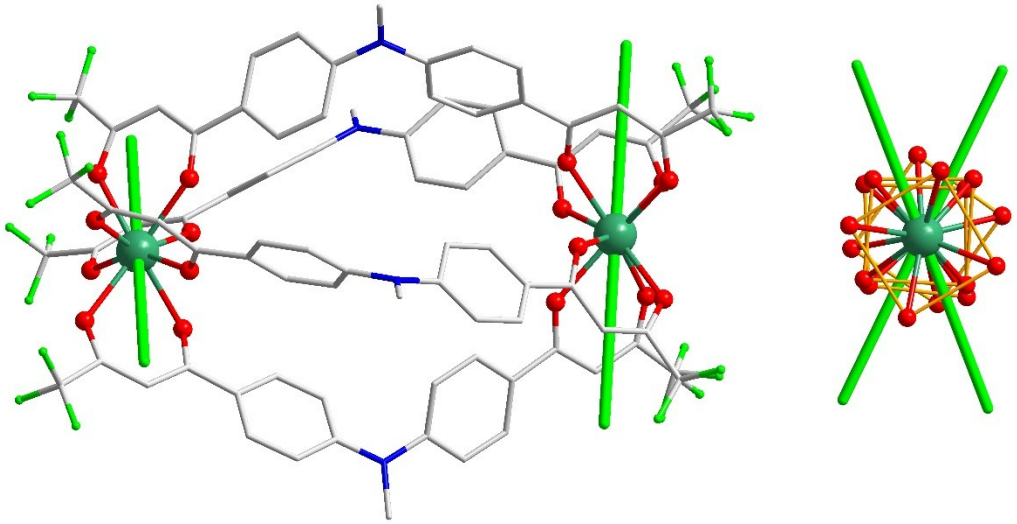

Fig. S16 Magnetic easy axis direction of each Dy(III) ion in **7** (left) and the side view (right).